AMERICAN SOCIETY FOR MICROBIOLOGY | mBio®

RESEARCH ARTICLE
Molecular Biology and Physiology

Mechanistic Understanding Enables the Rational Design of Salicylanilide Combination Therapies for Gram-Negative Infections

Janine N. Copp,[a,b] Daniel Pletzer,[c*] Alistair S. Brown,[a] Joris Van der Heijden,[b*] Charlotte M. Miton,[b] Rebecca J. Edgar,[a] Michelle H. Rich,[a*] Rory F. Little,[a] Elsie M. Williams,[a] Robert E. W. Hancock,[c] Nobuhiko Tokuriki,[b] David F. Ackerley[a,d]

[a]School of Biological Sciences, Victoria University of Wellington, Wellington, New Zealand
[b]Michael Smith Laboratories, University of British Columbia, Vancouver, Canada
[c]Center for Microbial Diseases and Immunity Research, Department of Microbiology and Immunology, University of British Columbia, Vancouver, Canada
[d]Centre for Biodiscovery, Victoria University of Wellington, Wellington, New Zealand

ABSTRACT One avenue to combat multidrug-resistant Gram-negative bacteria is the coadministration of multiple drugs (combination therapy), which can be particularly promising if drugs synergize. The identification of synergistic drug combinations, however, is challenging. Detailed understanding of antibiotic mechanisms can address this issue by facilitating the rational design of improved combination therapies. Here, using diverse biochemical and genetic assays, we examine the molecular mechanisms of niclosamide, a clinically approved salicylanilide compound, and demonstrate its potential for Gram-negative combination therapies. We discovered that Gram-negative bacteria possess two innate resistance mechanisms that reduce their niclosamide susceptibility: a primary mechanism mediated by multidrug efflux pumps and a secondary mechanism of nitroreduction. When efflux was compromised, niclosamide became a potent antibiotic, dissipating the proton motive force (PMF), increasing oxidative stress, and reducing ATP production to cause cell death. These insights guided the identification of diverse compounds that synergized with salicylanilides when coadministered (efflux inhibitors, membrane permeabilizers, and antibiotics that are expelled by PMF-dependent efflux), thus suggesting that salicylanilide compounds may have broad utility in combination therapies. We validate these findings *in vivo* using a murine abscess model, where we show that niclosamide synergizes with the membrane permeabilizing antibiotic colistin against high-density infections of multidrug-resistant Gram-negative clinical isolates. We further demonstrate that enhanced nitroreductase activity is a potential route to adaptive niclosamide resistance but show that this causes collateral susceptibility to clinical nitro-prodrug antibiotics. Thus, we highlight how mechanistic understanding of mode of action, innate/adaptive resistance, and synergy can rationally guide the discovery, development, and stewardship of novel combination therapies.

IMPORTANCE There is a critical need for more-effective treatments to combat multidrug-resistant Gram-negative infections. Combination therapies are a promising strategy, especially when these enable existing clinical drugs to be repurposed as antibiotics. We examined the mechanisms of action and basis of innate Gram-negative resistance for the anthelmintic drug niclosamide and subsequently exploited this information to demonstrate that niclosamide and analogs kill Gram-negative bacteria when combined with antibiotics that inhibit drug efflux or permeabilize membranes. We confirm the synergistic potential of niclosamide *in vitro* against a diverse range of recalcitrant Gram-negative clinical isolates and *in vivo* in a mouse abscess model. We also demonstrate that nitroreductases can confer resistance to niclosamide but show that evolution of these enzymes for enhanced niclosamide resistance confers a collateral sensitivity to other clinical anti-

Citation Copp JN, Pletzer D, Brown AS, Van der Heijden J, Miton CM, Edgar RJ, Rich MH, Little RF, Williams EM, Hancock REW, Tokuriki N, Ackerley DF. 2020. Mechanistic understanding enables the rational design of salicylanilide combination therapies for Gram-negative infections. mBio 11:e02068-20. https://doi.org/10.1128/mBio.02068-20.

Invited Editor Paul S. Hoffman, University of Virginia

Editor Nina R. Salama, Fred Hutchinson Cancer Research Center

Address correspondence to Janine N. Copp, janine.copp@msl.ubc.ca, or David F. Ackerley, david.ackerley@vuw.ac.nz.

* Present address: Daniel Pletzer, Department of Microbiology and Immunology, University of Otago, Dunedin, New Zealand; Joris Van der Heijden, Ottawa Virus Manufacturing Facility, Ottawa Hospital Research Institute, Ottawa, Canada; Michelle H. Rich, School of Biomolecular and Biomedical Sciences, O'Brien Centre for Science, University College Dublin, Dublin, Ireland.

Received 27 July 2020
Accepted 6 August 2020
Published 15 September 2020

biotics. Our results highlight how detailed mechanistic understanding can accelerate the evaluation and implementation of new combination therapies.

KEYWORDS synergy, repurposing, niclosamide, colistin, efflux, nitroreductase, resistance, proton motive force, antibiotic resistance, drug efflux

New therapeutic strategies are urgently required to combat multidrug-resistant (MDR) Gram-negative bacteria (1). The coadministration of two or more drugs (combination therapy) (2) is a promising approach, especially if the drugs exhibit synergy, i.e., enhanced efficacy over the predicted additive effects (3, 4). Synergistic combination therapies can kill microbes that are resistant to one of the drugs in the pair, may slow the evolution of resistance (5–7), and can facilitate the use of lower doses of each drug, thus reducing side effects and adverse reactions (8). The identification of synergistic drug combinations, however, is challenging due to the infrequency of synergistic relationships and the substantial scale of combinatorial drug screening (e.g., for a collection of 1,000 compounds, 499,500 pairwise combinations are possible, even before considering optimal relative concentrations) (3, 4). Mechanistic understanding of synergy may reveal novel antibiotic targets and guide the rational design of superior drug combinations, e.g., the coadministration of β-lactam compounds and β-lactamase inhibitors (9). However, for the majority of combination therapies the underlying basis of synergism is unclear. Indeed, despite clinical use for almost 50 years, the synergism of trimethoprim and sulfamethoxazole was only explored in detail in 2018 (10). Combination therapy may also enable compounds that have been clinically approved for other conditions, e.g., antidepressants, antipsychotics, and antidiarrhetics (11–13), to be repurposed as antibiotics; such compounds typically have detailed data available regarding their toxicity, formulation, and pharmacology that can expedite their clinical progression (14). However, the screening of clinical compounds for repurposing potential is laborious and often necessitates high-throughput robotic systems (13, 15). Detailed knowledge of the antibiotic mechanisms of action of promising clinical compounds would accelerate drug repurposing approaches and enable the circumvention of resistance mechanisms that may mask activity in initial screens. Thus, comprehensive understanding of both the mode of action and innate resistance mechanisms is important to inform the rational design of superior combination therapies that harness repurposed clinical compounds.

Niclosamide (Fig. 1a) is a clinically approved drug that has been used to treat helminth parasites in humans and animals for more than 50 years (16). Recently, several studies have suggested the potential of repurposing niclosamide for other medical applications; e.g., niclosamide appears to modulate metabolic disorders and neurological conditions and has antiproliferative effects against various cancers (17). The diverse pharmacological activities of niclosamide are likely the result of oxidative phosphorylation uncoupling and the modulation of signaling pathways (18, 19). Niclosamide exhibits antiviral activity against severe acute respiratory syndrome coronavirus (SARS-CoV) (20, 21) and is an effective antibiotic against Gram-positive and acid-fast pathogens (e.g., *Staphylococcus aureus*, *Clostridium difficile*, and *Mycobacterium tuberculosis*), as well as against *Helicobacter pylori* (22–25). As an anti-infective, the low absorption rate and poor oral bioavailability of niclosamide may hamper its use (26); however, optimized derivatives, nano-based formulations, and/or local administration may rescue its therapeutic potential (27–29). In isolation, niclosamide exhibits no activity against most Gram-negative pathogens (1, 23). Nevertheless, it was recently reported that *in vitro* coadministration of niclosamide and colistin can overcome colistin resistance in Gram-negative bacteria (30–32). While these findings suggest that niclosamide may hold cryptic antibiotic potential, the molecular basis that underlies its antibiotic mode of action and synergy and the lack of efficacy against Gram-negative bacteria has been hitherto unknown.

In this work, we examine the innate resistance mechanisms and antibacterial mode of action of niclosamide and related salicylanilide analogs, thus revealing their thera-

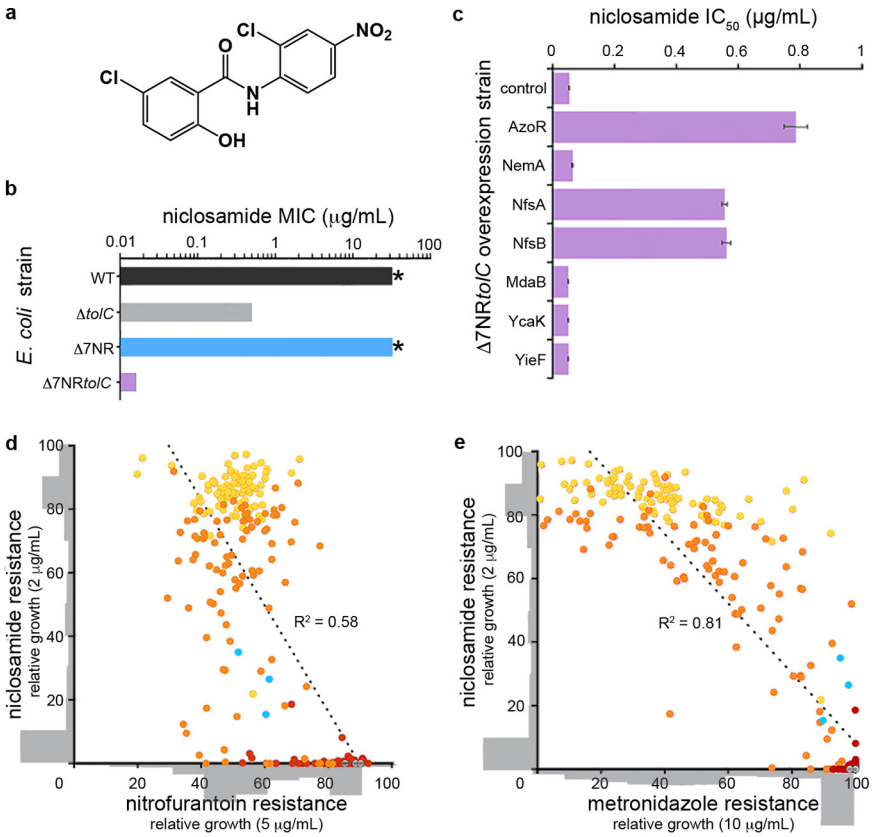

FIG 1 Niclosamide resistance mechanisms. (a) Structure of niclosamide. (b) MIC of *E. coli* wild-type (WT), Δ*tolC*, Δ7NR, and Δ7NR*tolC* strains. Asterisks (*) indicate >32 μg · ml^{-1}, which is the solubility limit of niclosamide in growth media. (c) IC_{50} analysis of Δ7NR*tolC* strains individually overexpressing candidate *E. coli* nitroreductases or a vector-only control following niclosamide administration. Error bars indicate standard errors of the means (SEM). (d and e) Covariance plots displaying the interrelated profiles of niclosamide, metronidazole, and nitrofurantoin resistance. A total of 90 colonies of NfsA variants were picked from agar plates without niclosamide (red) or with 0.2 μg · ml^{-1} niclosamide (orange) or 2 μg · ml^{-1} niclosamide (yellow). Variants were grown overnight and then screened for niclosamide resistance (growth at 2 μg · ml^{-1}) and (d) nitrofurantoin resistance or (e) metronidazole resistance (growth at 5 or 10 μg · ml^{-1}, respectively). Variant distribution is shown as gray histograms that are overlaid on the *x* and *y* axes. R^2 values (linear regression analysis) are displayed; $P < 0.01$. *E. coli* NfsA and vector-only controls are displayed in cyan and gray, respectively. All panels are constructed from pooled data from at least three independent biological replicates.

peutic potential as potent antibiotics when utilized in rationally designed combination therapies. We reveal a potential route to adaptive niclosamide resistance but demonstrate that this leads to collateral susceptibility; thus, the emergence of resistance via this route may be prevented or slowed in the clinic. In addition, we demonstrate the *in vitro* efficacy of niclosamide combination therapy against MDR Gram-negative clinical isolates and confirm synergy *in vivo* using a murine abscess model and high-density infections that mimic a clinical situation where antibiotics typically fail (33).

RESULTS

TolC-mediated efflux and nitroreductases (NRs) confer innate niclosamide resistance in *E. coli*. To investigate the mechanisms by which *Escherichia coli* mitigates the antibiotic potential of niclosamide, we first examined multidrug efflux pumps, which represent a dominant *E. coli* resistance mechanism to expel toxic compounds (34). We tested a variety of *E. coli* strains that lacked individual components of the three major tripartite efflux systems to ascertain whether efflux contributed to niclosamide resistance. In total, nine individual gene deletions were investigated for their effect on niclosamide MIC (see Table S1 in the supplemental material). Notably, deletion of the gene encoding the outer membrane channel TolC (Δ*tolC*) reduced MIC by >64-fold

(MIC = 0.5 $\mu g \cdot ml^{-1}$), whereas no other deletions had any effect (MIC of >32 $\mu g \cdot ml^{-1}$; Table S1). This result suggests that TolC-mediated efflux is one of the predominant mechanisms of niclosamide resistance. Interestingly, deletion of genes encoding other components of the principal resistance-nodulation-division (RND)-type TolC tripartite complex (AcrA or AcrB) had no effect on MIC. This was likely due to TolC interacting with alternative efflux components such as AcrE or AcrF, resulting in alternative niclosamide-capable pump assemblies (34).

Next, we explored the role of azoreductase and nitroreductase (NR) flavoenzymes in niclosamide susceptibility, due to their importance in diverse metabolic pathways, including antibiotic metabolism (35, 36). Although previous antibiotic metabolism studies had primarily focused on the bioreductive activation of nitro-prodrugs, here we considered that there was potential for nitroreduction to be a detoxifying mechanism as there is evidence that the nitro-moiety of niclosamide is an important structural feature for uncoupling activity (37). To test this, we utilized an *E. coli* strain that lacked seven flavoenzyme genes with confirmed or putative nitroreductase or azoreductase activity (Δ7NR) (38) (Table S1). Although niclosamide resistance in the Δ7NR strain did not change compared to wild-type *E. coli* (MIC of >32 $\mu g \cdot ml^{-1}$), an otherwise isogenic strain that also lacked TolC (Δ7NR*tolC*) was 2,000-fold more susceptible to niclosamide than the wild-type strain (MIC = 0.016 $\mu g \cdot ml^{-1}$) and 32-fold more susceptible than the Δ*tolC* strain (Fig. 1b; see also Table S1). The relative contributions of each of the seven flavoenzymes were delineated by individually overexpressing the corresponding genes in the Δ7NR*tolC* strain and investigating their effects on niclosamide IC_{50} (the concentration of niclosamide required to reduce the bacterial burden by 50%). We demonstrated that three enzymes, NfsA, NfsB, and AzoR, increased niclosamide IC_{50} by 10-fold to 15-fold (Fig. 1c). Although these three enzymes derive from two distinct structural folds, they are all proficient nitroreductases (38). To confirm the effect of nitroreduction on the antimicrobial activity of niclosamide, we investigated the terminal nitroreduction product (39), amino-niclosamide. The Δ*tolC* and Δ7NR*tolC* strains exhibited amino-niclosamide MICs of 20 $\mu g \cdot ml^{-1}$ (see Fig. S1 in the supplemental material); i.e., amino-niclosamide was 40-fold and 1,250-fold less toxic to the Δ*tolC* and Δ7NR*tolC* strains than niclosamide, respectively. No toxicity could be detected against the wild-type and Δ7NR strains (MIC of >160 $\mu g \cdot ml^{-1}$). Increasing nitroreductase activity could therefore be a potential adaptive strategy for bacteria to develop resistance against niclosamide. We hypothesized, however, that this might cause collateral sensitivity to nitroaromatic prodrug antibiotics such as nitrofurantoin and metronidazole. To test this hypothesis, we selected Δ7NR*tolC* cells expressing different NfsA variants (generated via multisite saturation mutagenesis to combinatorically randomize seven active-site residues) for resistance to either 0.2 or 2 $\mu g \cdot ml^{-1}$ niclosamide and then counterscreened for sensitivity to nitrofurantoin or metronidazole. Consistent with our hypothesis, increasing niclosamide resistance via more-proficient nitroreductase variants concomitantly decreased nitrofurantoin and metronidazole resistance (Fig. 1d and e).

Niclosamide disrupts oxidative phosphorylation in *E. coli*. Next, the underlying mechanisms of niclosamide antibiotic activity were investigated. As previous studies have demonstrated that niclosamide uncouples oxidative phosphorylation in mitochondria, *C. difficile*, and *H. pylori* (18, 24, 25), multiple physiological attributes were explored that relate to this process in Gram-negative bacteria, namely, proton motive force (PMF), oxygen consumption, ATP production, and redox homeostasis. The PMF has two parameters: the electric potential ($\Delta\Psi$) and the transmembrane proton (ΔpH) gradients. First, the effect of niclosamide on PMF dissipation was investigated in EDTA-permeabilized *E. coli* using a fluorescent assay that employs the membrane potential-sensitive dye $diSC_3(5)$—a caged cation that distributes in the membrane according to $\Delta\Psi$ and self-quenches. We observed that niclosamide specifically dissipated the $\Delta\Psi$ (Fig. 2a) as revealed by dequenching of $diSC_3 5$ fluorescence.

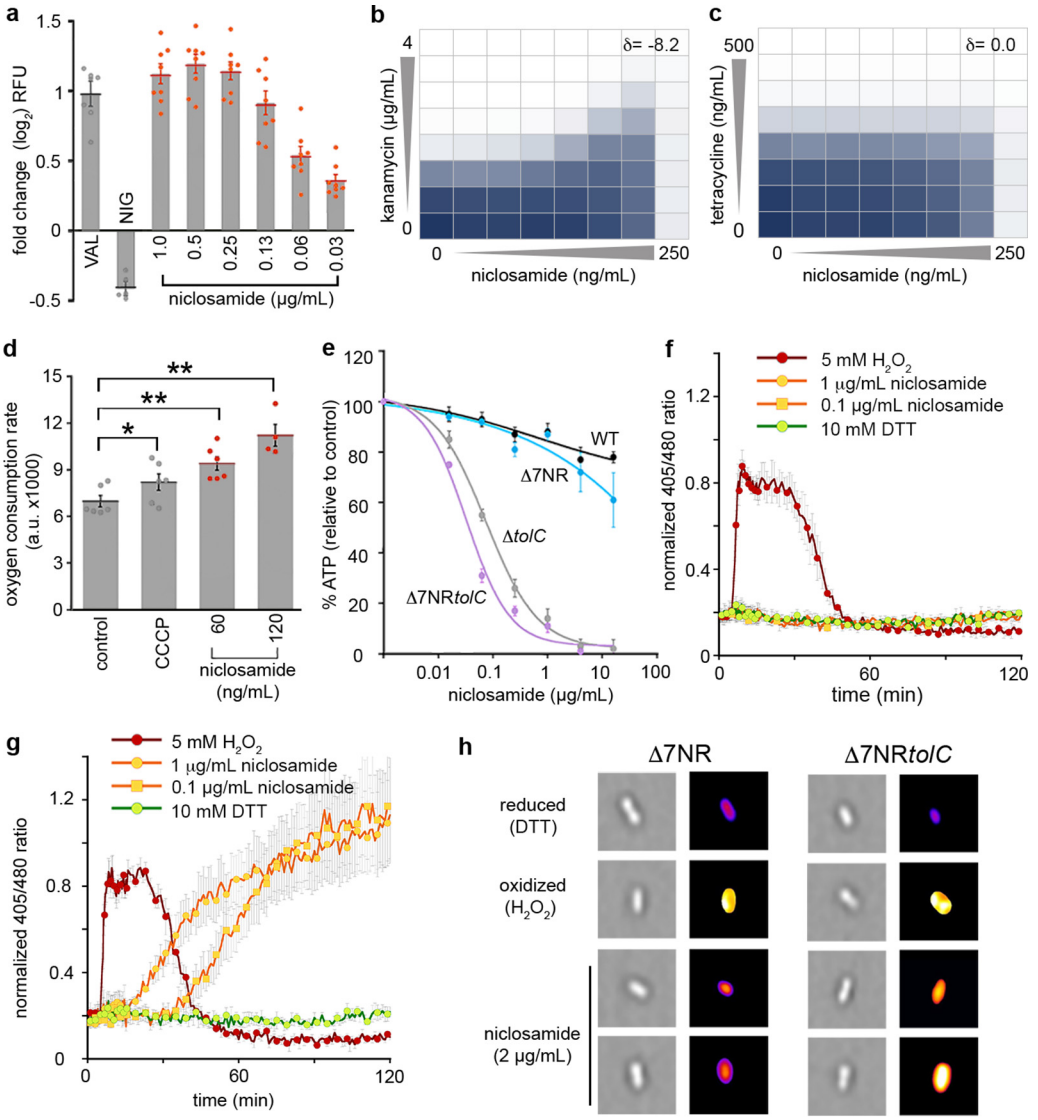

FIG 2 Antibiotic mechanisms of niclosamide. (a) Fold change in $DiSC_3(5)$ fluorescence. *E. coli* was grown in MHB with 10 mM EDTA to an OD_{600} of 1. Cells were incubated with $DiSC_3(5)$ for 20 min prior to administration of 0.5 μg/ml valinomycin (VAL; a $\Delta\Psi$-dissipating ionophore), 0.5 μg/ml nigericin (NIG; a ΔpH-dissipating ionophore), or 0.03 to 1 μg/ml niclosamide. KCl (100 mM) was added to cells prior to valinomycin treatment. RFU, relative fluorescence units. (b and c) The combined inhibitory effects of 0 to 250 ng · ml^{-1} niclosamide and either (b) 0 to 4 μg · ml^{-1} kanamycin or (c) 0 to 500 ng · ml^{-1} tetracycline were tested against the Δ7NR*tolC* strain in a checkerboard format. Bacterial growth is shown as a heat plot. (d) Oxygen consumption was measured using the MitoXpress oxygen probe in Δ7NR*tolC* cells (mid-log phase; $OD_{600} = 0.15$) overlaid with mineral oil for 20 min. a.u., arbitrary units. (e) Relative cellular ATP levels were estimated by luciferase activity and compared to an unchallenged (DMSO-only) control. (f and g) Intracellular oxidation levels were measured in (f) WT *E. coli* and (g) Δ*tolC* strains constitutively expressing redox-sensitive GFP (roGFP) following administration of 5 mM H_2O_2 (oxidized control), 10 mM DTT (reduced control), or niclosamide. (h) Representative high-throughput fluorescence microscopy images of Δ7NR and Δ7NR*tolC* cells 120 min after administration of DTT, H_2O_2, or niclosamide. Images on the right are pseudocolored ratio images after analysis with ImageJ. Panels a to g were constructed from pooled data from at least three independent biological replicates. Labels indicate significant responses over the control (* = $P < 0.05$; ** = $P < 0.01$). Statistical analyses were performed using one-way analysis of variance (ANOVA) and the Kruskal-Wallis test. Error bars indicate SEM.

Next, to confirm this result, checkerboard assays (dose response growth assays using serial dilutions of two drugs in combination) were performed in the Δ7NR*tolC* strain using niclosamide and antibiotics that rely upon either $\Delta\Psi$ or ΔpH for cell uptake (kanamycin or tetracycline, respectively). The fractional inhibitory concentration index is frequently used to characterize drug interactions but has limitations with respect to analyzing compounds for which an individual MIC cannot be obtained (here, niclos-

amide). Thus, drug interactions were analyzed via zero interaction potency (ZIP) scores (δ) that quantify the change in dose-response curves between individual drugs and combinations thereof from the expectation of no interaction; δ scores of >0 indicate synergism, a score of 0 indicates no interaction, and scores of <0 indicate antagonism (40). Kanamycin efficacy was reduced in the presence of niclosamide; i.e., niclosamide was antagonistic when coadministered with kanamycin, corresponding to a δ score of -8.2 (Fig. 2b), which is consistent with $\Delta\Psi$ dissipation undermining $\Delta\Psi$-dependent kanamycin uptake. In contrast, tetracycline efficacy was not affected by niclosamide coadministration ($\delta = 0.0$; Fig. 2c), as tetracycline relies upon ΔpH for uptake (Fig. 2b and c). PMF disruption can reduce ATP production and increase both oxygen consumption and oxidative stress (41). We therefore confirmed that niclosamide administration significantly increased oxygen consumption in the Δ7NR*tolC* strain (by 1.4-fold and 1.6-fold after administration of 60 ng $\cdot$ ml^{-1} and 120 ng $\cdot$ ml^{-1} niclosamide, respectively; Fig. 2d). Niclosamide administration caused reductions of the cellular ATP concentrations to 3% and 1% of the dimethyl sulfoxide (DMSO)-control concentrations when 4 μg $\cdot$ ml^{-1} niclosamide was administered to the Δ*tolC* and Δ7NR*tolC* strains, respectively (Fig. 2e). Employing strains constitutively expressing redox-sensitive green fluorescent protein (roGFP) (42), we determined that niclosamide also disrupted redox homeostasis in the Δ*tolC* and Δ7NR*tolC* strains, causing an increase in oxidative stress (Fig. 2f and g; see also Fig. S1). Next, using high-throughput fluorescence microscopy, increased intracellular oxidative stress was visualized in Δ7NR*tolC* cells following niclosamide administration. The distribution of redox stress per cell was plotted as histograms (Fig. S2), and a random selection of pseudocolored ratio images are presented in Fig. 2h. In strains that retained TolC function, niclosamide did not have a significant effect on cellular ATP levels, oxygen consumption, or redox homeostasis. Taken together, these data suggest that, when efflux is compromised, niclosamide dissipates the $\Delta\Psi$ to collapse the PMF and uncouple oxidative phosphorylation in *E. coli*.

Niclosamide synergizes with efflux pump inhibitors and membrane permeabilizers for enhanced efficacy against *E. coli*. After establishing the mode of action of niclosamide and the basis of Gram-negative innate resistance, we next sought to identify compounds that sensitize Gram-negative bacteria to niclosamide when administered in combination. Predicting that efflux pump inhibitors such as phenylalanine-arginine β-naphthylamide (PAβN) (43) would increase niclosamide sensitivity, checkerboard assays were employed to screen niclosamide and PAβN against *E. coli*. Considerable synergy was observed ($\delta = 47.9$; Fig. 3a). It was next reasoned that increased niclosamide influx via outer membrane permeabilization might mitigate TolC-mediated efflux. Therefore, membrane permeabilizing polymyxin antibiotics were investigated for synergy and, consistent with recent reports (30–32), synergy was observed when colistin or polymyxin B was coadministered with niclosamide ($\delta = 28.1$ or 25.6, respectively) (Fig. 3b and c). We hypothesized that synergism was due to the cascading effect of the mode of action of niclosamide, in that polymyxins increased the influx of niclosamide and thereby facilitated PMF dissipation, which in turn compromised the efficiency of PMF-dependent niclosamide efflux (as efflux was dependent upon PMF [44]). Ultimately, this would result in higher intracellular concentrations of niclosamide and thus in enhanced antibiotic effects (Fig. 4). Indeed, polymyxin synergy was less evident in the Δ*tolC* strain ($\delta = 7.6$ and 9.7 for colistin and polymyxin B, respectively; Fig. 3d and e) and niclosamide administration inhibited efflux in EDTA-permeabilized *E. coli* (observed via increasing intracellular accumulation of the fluorescent nucleic acid probe Hoechst 33342; Fig. S1).

Oxyclozanide potentiates diverse antibiotics, likely via inhibition of PMF-dependent efflux. Next, it was examined whether the synergistic relationships observed as described above were maintained for other halogenated salicylanilides, namely, oxyclozanide, closantel, and rafoxanide. It was confirmed that all these niclosamide analogs synergized with both PAβN and colistin ($\delta = 21.5$ to 49.8; Fig. 3f; see also Fig. S3). Of note, the relatively high solubility of oxyclozanide in growth media ($\sim$512 μg $\cdot$ ml^{-1}), compared to that of other salicylanilides ($\sim$64 μg $\cdot$ ml^{-1}), enabled

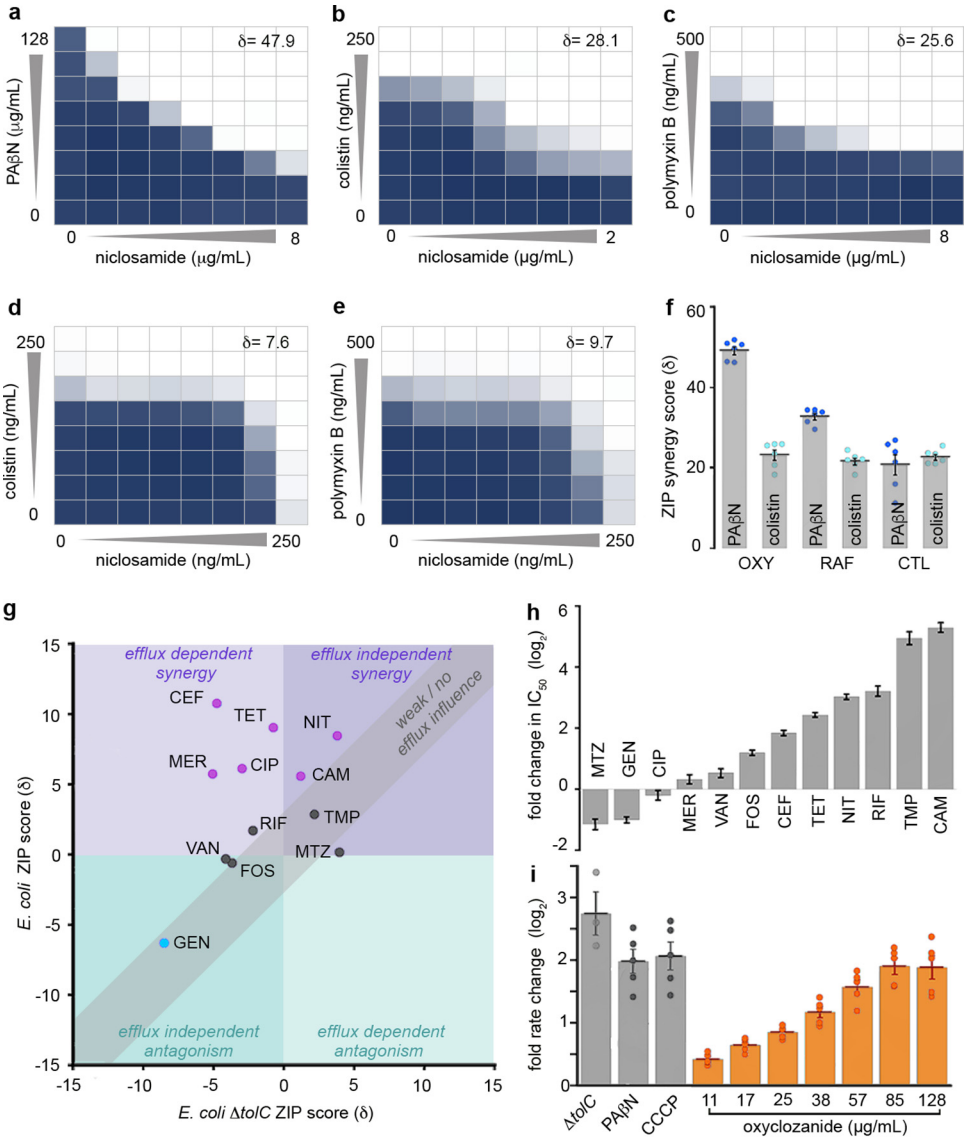

FIG 3 Analyses of salicylanilide synergy interactions. (a to c) The combined inhibitory effects of 0 to 8 μg · ml^{-1} niclosamide and (a) 0 to 128 μg · ml^{-1} PAβN or (b) 0 to 250 ng · ml^{-1} colistin or (c) 0 to 500 ng · ml^{-1} polymyxin B were tested against *E. coli* using checkerboard analysis. ZIP synergy scores (δ) are presented. Bacterial growth is depicted as a heat plot. (d and e) The combined inhibitory effects of 0 to 250 ng · ml^{-1} niclosamide and either (d) 0 to 250 ng · ml^{-1} colistin or (e) 0 to 500 ng · ml^{-1} polymyxin B were tested against *E. coli* Δ*tolC* in checkerboard analyses. Bacterial growth is depicted as a heat plot. (f) A bar graph of ZIP scores (δ) depicting the synergism of oxyclozanide (OXY), rafoxanide (RAF), or closantel (CTL) in combination with PAβN or colistin against *E. coli*. Error bars indicate SEM. (g and h) Analysis of oxyclozanide synergy with nitrofurantoin (NIT), metronidazole (MTZ), cefotaxime (CEF), rifampin (RIF), tetracycline (TET), gentamicin (GEN), ciprofloxacin (CIP), chloramphenicol (CAM), trimethoprim (TMP), fosfomycin (FOS), meropenem, (MER) or vancomycin (VAN). (g) A covariance plot of antibiotic ZIP scores from checkerboard assays conducted in minimal media with oxyclozanide against *E. coli* and *E. coli* Δ*tolC*. (h) A bar chart displaying fold changes of IC_{50} values in the Δ*tolC* strain compared to the *E. coli* WT strain; uncertainty is indicated by error bars. (i) Fold change in the rate of Hoechst 33342 fluorescence (compared to a DMSO control) in Δ*tolC* cells or WT *E. coli* following administration of 28 μg · ml^{-1} PAβN, 5 μg · ml^{-1} CCCP, or 11.2 to 128 μg · ml^{-1} oxyclozanide. Error bars indicate SEM. All panels were constructed from pooled data from at least three independent biological replicates.

the observation of an oxyclozanide MIC (256 μg · ml^{-1}); i.e., sufficiently high concentrations of oxyclozanide were able to overcome TolC-mediated efflux. Since moderate synergistic relationships can be detected only at concentrations nearing the MIC of both drugs and are emphasized in bacterial cultures under conditions of nutrient limitation (45), oxyclozanide checkerboard assays in minimal media were used to identify additional antibiotics that interact with salicylanilides against *E. coli*. Twelve

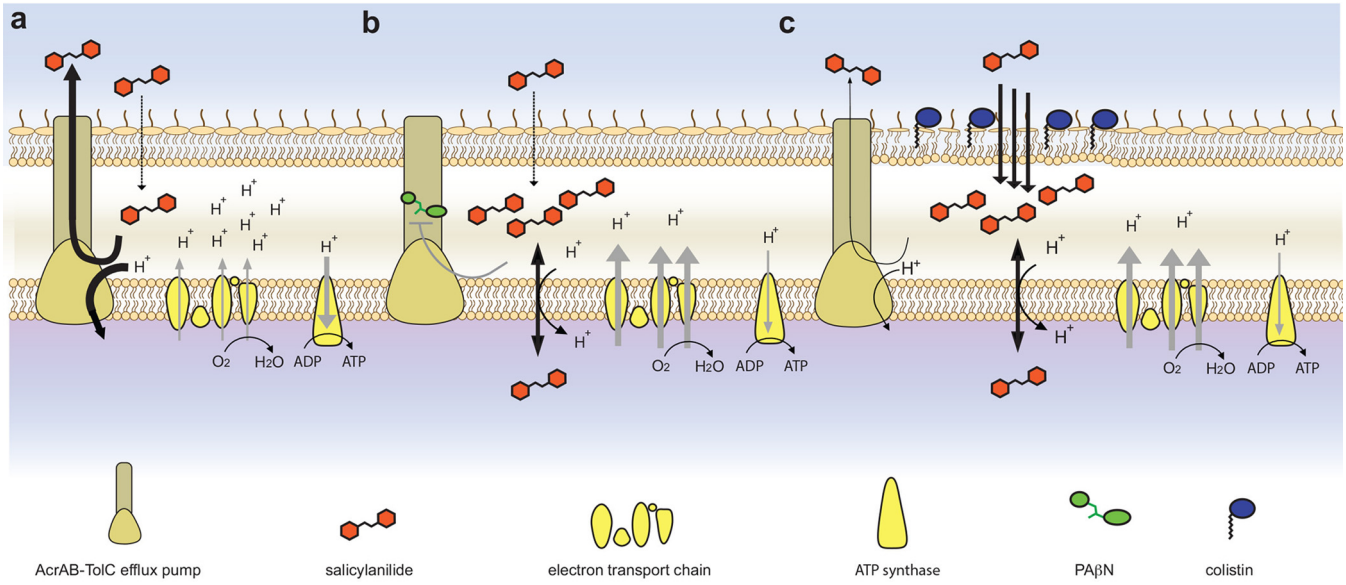

FIG 4 Proposed salicylanilide mechanisms of action. (a) Salicylanilide crosses the outer membrane but is expelled from the cell via (PMF-dependent) TolC-mediated efflux; electron transport, membrane polarization, oxygen consumption, and ATP synthesis are not affected. (b) When TolC is inhibited by compounds such as PAβN, salicylanilides uncouple the electron transport chain, dissipate the PMF, increase oxygen consumption, and decrease ATP production. (c) When the outer membrane is disrupted via compounds such as colistin, salicylanilides rapidly enter the cell, overwhelming TolC-mediated efflux, uncoupling the electron transport chain, dissipating the PMF (inhibiting PMF-dependent efflux), increasing oxygen consumption, and decreasing ATP production.

antibiotics with diverse cellular targets (Table S1) were examined. Interestingly, 6 of 12 antibiotics synergized with oxyclozanide (chloramphenicol, tetracycline, cefotaxime, meropenem, ciprofloxacin, and nitrofurantoin; $\delta = 5.7$ to 10.8), 5 antibiotics displayed no or weak interactions ($\delta = -0.6$ to 2.9) and, consistent with the dependence of aminoglycosides on $\Delta\Psi$ for uptake, oxyclozanide antagonized gentamicin activity ($\delta = (\delta = -6.3)$ (Fig. 3g; see also Table S2). These combinatorial effects were found to have been neutralized or reversed in the Δ*tolC* strain (Fig. 3g; see also Table S2), and oxyclozanide synergy was typically stronger for the antibiotics that are TolC substrates (indicated by fold IC_{50} change in the Δ*tolC* strain compared to wild-type *E. coli*; Fig. 3h). These results suggest that oxyclozanide synergy might be at least partially underpinned by the inhibition of efflux via PMF dissipation (Fig. 4). To substantiate this hypothesis, the effect of oxyclozanide on cellular efflux was examined using Hoechst 33342. Indeed, administration of oxyclozanide inhibited efflux (Fig. 3i). Taken together, these results demonstrate that chemical disruption of TolC-mediated efflux or membrane integrity sensitizes *E. coli* to salicylanilides. Further studies are required to explain the details of the drug interactions; however, our results suggest that PMF-dissipating compounds such as salicylanilides may potentiate the activity of diverse antibiotics through the disruption of efflux.

Niclosamide/colistin combination therapy is effective against diverse clinical Gram-negative isolates *in vitro* and *in vivo*. Finally, we investigated the potential of salicylanilide combination therapy against a range of Gram-negative clinical isolates. Due to the immediate repurposing potential of niclosamide as an FDA-approved clinical drug and increasing concerns around colistin-resistant pathogens, we prioritized these two compounds. Checkerboard assays were performed on nine MDR clinical isolates across diverse phyla, including *Acinetobacter*, *Pseudomonas*, and the *Enterobacteriaceae* (Table S3). Coadministration of niclosamide and colistin yielded synergistic efficacy in all strains ($\delta = 8.4$ to 42.6), including colistin-resistant clinical isolates, *Pseudomonas aeruginosa* LESB58, *Acinetobacter baumannii* C4, and *E. coli* NCTC13846, enabling the use of up to 8-fold-lower doses of colistin (Fig. 5a; see also Fig. S5), which is of particular importance due to the nephrotoxicity issues associated with this antibiotic (46).

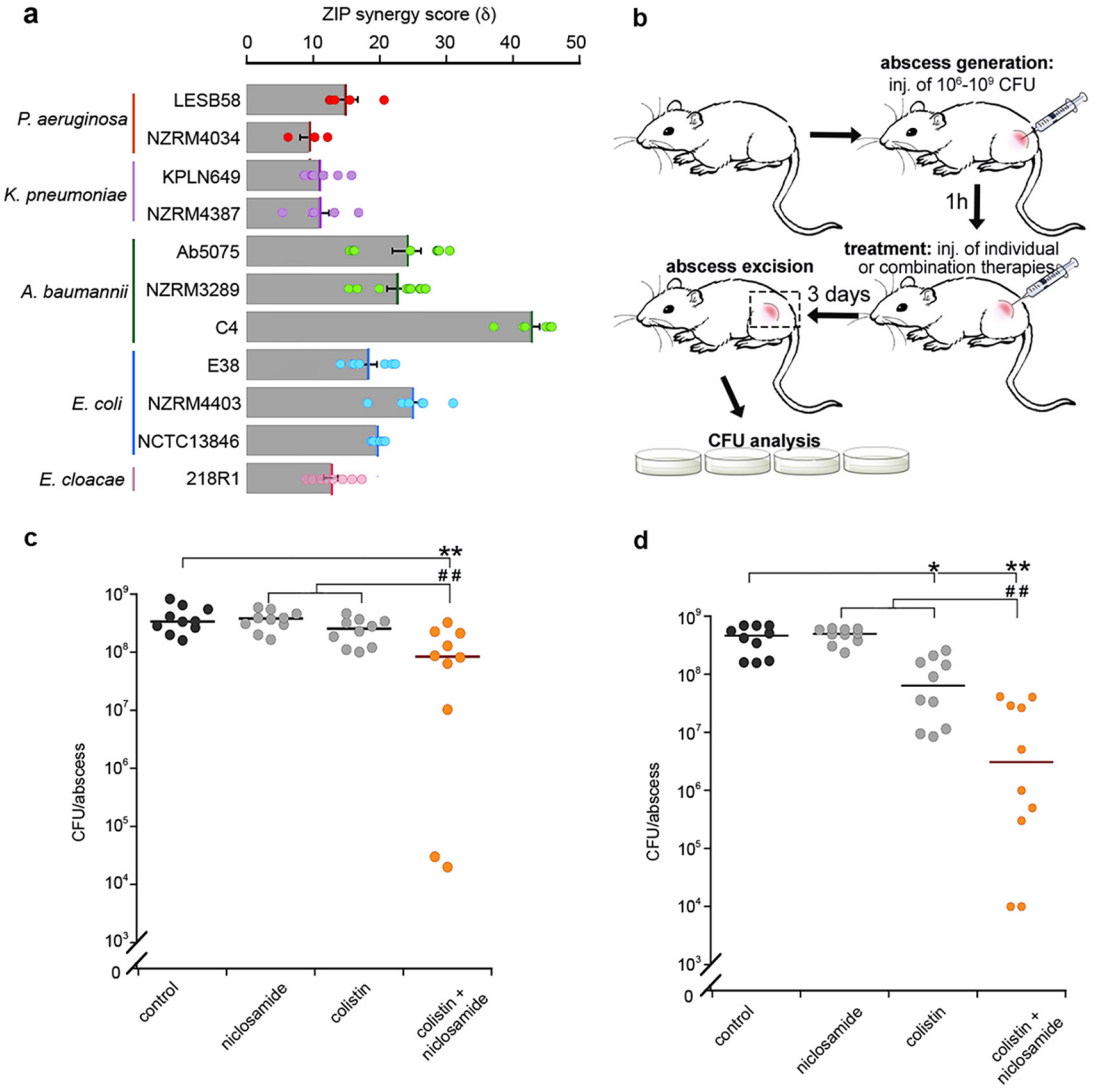

FIG 5 Niclosamide/colistin combination therapy was effective against recalcitrant MDR Gram-negative strains. (a) Bar graph depicting *in vitro* ZIP scores (δ) of niclosamide and colistin coadministration against the following clinical MDR Gram-negative strains: *P. aeruginosa* LESB58, *P. aeruginosa* NZRM4034, *K. pneumoniae* KPLN649, *K. pneumoniae* NZRM4387, *A. baumannii* Ab5075, *A. baumannii* NZRM3289, *A. baumannii* C4, *E. coli* E38, *E. coli* NZRM4403, *E. coli* NCTC 13846, and *E. cloacae* 218R1. The ZIP synergy score (δ) represents the average of interaction data from an 8-by-8 dose-response matrix. Data were averaged from at least three independent experiments, and error bars indicate SEM. (b) Diagram of abscess model procedure and analysis. inj., injection. (c and d) Dot plots of (c) colistin-resistant *P. aeruginosa* LESB58 and (d) *K. pneumoniae* KPLN649 survival, represented as CFU recovered per abscess after administration of 10 mg · kg^{-1} niclosamide ethanolamine salt and 0.15 mg · kg^{-1} (*P. aeruginosa*) or 2.5 mg · kg^{-1} (*K. pneumoniae*) colistin as individual or combined therapeutics. Labels indicate significant responses over the PEG control (*, $P < 0.05$; **, $P < 0.01$) or synergistic responses, i.e., significant differences measured for the combination therapy over the sum of the effects of each agent alone (##, $P < 0.01$). Statistical analyses were performed using one-way analysis of variance (ANOVA) and the Kruskal-Wallis test with Dunn's correction (two sided).

The poor bioavailability and pharmacology of niclosamide may be mitigated via local administration, e.g., topical or inhalation therapies (29, 47). Here, we examined the *in vivo* antibacterial synergy of niclosamide via direct injection in a high-density murine cutaneous infection model that mimics clinical situations where antibiotic treatments are typically unsuccessful, e.g., skin abscesses (33) (Fig. 5b). The synergistic efficacy of niclosamide and colistin was validated against *P. aeruginosa* LESB58 and *Klebsiella pneumoniae* KPLN649. Coadministration resulted in significant synergistic efficacy against both strains, reducing the *K. pneumoniae* and *P. aeruginosa* bacterial loads by 32-fold and 12-fold, respectively, over the sum of the individual therapies, and by 239-fold and 19-fold, respectively, compared to levels seen with vehicle-only controls

(Fig. 5c and d). This is the first report of *in vivo* efficacy for niclosamide and colistin against Gram-negative pathogens, and notably, this was achieved against recalcitrant high-density infections for which no effective clinical treatments currently exist (33). It is also important that this study was focused on detecting niclosamide/colistin synergy rather than identifying the best formulation or dose ratio for efficacy; more-significant efficacy could likely be achieved by optimizing the drug concentrations or dosing regimen.

DISCUSSION

By harnessing a diverse set of biochemical and genetic tools, this work explores the Gram-negative antibacterial potential of niclosamide and related salicylanilide analogs. We examine the molecular action of salicylanilides against Gram-negative bacteria, detailing not only the underlying mechanisms of antibiotic activity but also the basis for innate and adaptive resistance and the mechanisms that underpin the synergies between salicylanilides and a diversity of other antibiotics. These data enabled the development of a model that substantially advances our knowledge of the physiological effects of salicylanilides in Gram-negative bacteria (Fig. 4). Efflux is an established Gram-negative resistance mechanism, and, indeed, this is the predominant basis for niclosamide resistance. However, we demonstrate that salicylanilides also inhibit efflux and thus synergize with a wide range of antibiotics for which efflux is a common resistance mechanism. These data highlight the potential of the salicylanilide chemical scaffold, and of PMF-dissipating compounds in general, for the discovery and design of novel antibiotic adjuvants to address efflux-mediated resistance. We consider PMF dissipation, traditionally avoided in early drug development due to presumed toxicity, a promising and unexplored trait for the development of antimicrobials (48). Interestingly, many clinical compounds for diverse medical purposes have been reported to have mild PMF-dissipating activity and, in addition, some have displayed antibiotic efficacy against Gram-positive or acid-fast pathogens such as *S. aureus* and *M. tuberculosis* (48, 49). Gram-negative pathogens, in contrast, resist the action of such compounds via their robust cellular envelope and diverse efflux pumps (34). Coadministration of PMF-dissipating compounds with drugs that target efflux and cell permeability may therefore be a promising avenue to discover more-effective combination therapies. Combining mechanistic insights with previously established data around safety and pharmacology for repurposed "nonantibiotic" clinical compounds may rapidly identify attractive candidates for accelerated clinical development.

Understanding the evolutionary basis of antibiotic resistance is important to inform the sustainable use of next-generation antibiotics. Due to the failure of laboratory evolution experiments to generate niclosamide resistance in *S. aureus* or *H. pylori*, previous reports have suggested that a key advantage of niclosamide as a potential antimicrobial is the apparent lack of resistance mechanisms (25, 47). We show, however, that nitroreductases inactivate niclosamide to reduce antibiotic toxicity and that enhanced nitroreductase activity can cause niclosamide resistance. While modulation of nitroreductase activity is a known Gram-negative resistance mechanism against nitro-antibiotic compounds, this is typically caused by null mutations, i.e., genetic changes that result in a nonfunctional nitroreductase, to prevent the activation of prodrug antibiotics such as metronidazole (50). Our results suggest that resistance has the potential to emerge in the clinic through enhanced nitroreductase activity. Significantly, we show that this may result in collateral sensitivity to nitroimidazole antibiotics; thus, we propose a strategy to mitigate this evolutionary route, i.e., cyclic treatments of metronidazole. This demonstrates how mechanistic understanding can accelerate not only the discovery but also potentially the sustainability of new Gram-negative combination therapies.

In summary, we reveal the detailed mechanisms that underlie the antibiotic mode of action, routes of resistance, and synergistic relationships of salicylanilides. The results guided the discovery of novel combination therapies and emphasize how mechanistic understanding is critical when seeking to repurpose clinical compounds. Salicylanilides,

and likely other PMF-dissipating compounds, may have broad utility as Gram-negative antibiotics in combination therapies.

MATERIALS AND METHODS

Bacterial strains. *E. coli* BW25113 strains bearing individual gene deletions were obtained from the Keio knockout collection (51). Δ7NR and Δ7NR*tolC* mutants were generated via sequential knockout as previously described (52). New Zealand clinical isolates used in this study were *A. baumannii* NZRM3289, *P. aeruginosa* NZRM4034, *K. pneumoniae* NZRM4387, and *E. coli* NZRM4403 (obtained from the New Zealand Reference Culture Collection, Environmental Science and Research Ltd.). *K. pneumoniae* KPLN649, *A. baumannii* Ab5075, *P. aeruginosa* LESB58, *Enterobacter cloacae* 218R1, *E. coli* E38 (serotype O78:H-) (BEI Resources, NR-17717), *E. coli* NCTC 13846, and *A. baumannii* C4 were previously described (53, 54).

***In vitro* growth analyses.** MICs were determined using 2-fold dilutions, and growth was measured after 16 to 48 h (55). The MIC was the concentration that inhibited growth >90% compared to controls. DMSO was present at a final concentration of 2.5% unless otherwise stated. For checkerboard analysis, an 8-by-12 matrix was created with 2-fold serial dilutions of each compound. Bacterial colonies were isolated from a freshly streaked plate and resuspended in Mueller-Hinton broth (MHB) media for normalization using the optical density at 600 nm (OD_{600}). After addition of bacteria to reach a final OD_{600} of 0.001, checkerboard plates were incubated at 30°C with shaking for 16 h (or for 36 h at 37°C for *P. aeruginosa* strains), at which time the OD_{600} was measured. Checkerboard assays in minimal media were typically performed at 37°C (oxyclozanide checkerboard assays with nitrofurantoin, rifampin, tetracycline, and chloramphenicol were performed at 30°C) with shaking for 16 h, from a starting OD_{600} of 0.04. For the analysis of nitroreductase overexpression strains, individual colonies were transferred via a nitrocellulose membrane to an agar plate containing 1 mM IPTG (isopropyl-β-D-thiogalactopyranoside) and incubated for 3.5 h. IPTG-induced cells were then removed from the membrane and resuspended in MHB media for checkerboard analysis as described above. Relative IC_{50} values (the concentrations of the compound required to reduce the bacterial burden by 50% compared to unchallenged controls) were calculated from the dose-response curves using the four-parameter equation $y = m1 + (m2 - m1)/[1 + (x/m3)\text{^}m4]$ determined by Kaleidagraph software (Synergy Software, Reading, PA) where m1 = lower asymptote, m2 = lower asymptote, m3 = relative IC_{50} value, and m4 = slope.

Generation and screening of mutagenized NfsA variants. A plasmid-based multisite saturation mutagenesis library of *E. coli* NfsA (UniProtKB identifier [ID] P17117) was generated via combinatorial randomization of the codons encoding the following seven key active-site residues: S41, F42, F83, K222, S224, R225, and F227 (see Fig. S6 in the supplemental material). All codons were randomized to NDT (a degeneracy that specifies a balanced range of 12 different amino acids, including the native residue), with the exception of position 222, which was randomized to NNK (specifying all 20 possible amino acids). The resulting library of nearly 96 million codon variants was expressed in the Δ7NR*tolC* mutant. To analyze the activity of NfsA variants, library subsets were selected on agar plates using 0, 0.2, and 2 $\mu g \cdot ml^{-1}$ of niclosamide. Ninety colonies from each subset were subsequently screened via growth assays with niclosamide, metronidazole, and nitrofurantoin at 2, 10, and 5 $\mu g \cdot ml^{-1}$, respectively; growth was measured via OD_{600} following 4 h of incubation as previously described (56).

Synergy calculations. For each checkerboard analysis, an 8-by-8 matrix of averaged checkerboard results from at least three (typically >5) independent experiments was used to calculate ZIP scores using SynergyFinder (https://www.bioconductor.org/) (40, 57).

$DiSC_3(5)$ assay. Subcultures of *E. coli* BW25113 were grown to late exponential phase (OD_{600} of ~1) in MHB with 10 mM EDTA [to facilitate $DiSC_3(5)$ cell entry]. Cells were harvested by centrifugation, washed twice in buffer (5 mM HEPES [pH 7.2], 20 mM glucose, 5% DMSO), and then resuspended in buffer to a final OD_{600} of 0.085 with 1 μM DiSC3(5). For valinomycin, 100 mM KCl was added to the cell suspension containing $DiSC_3(5)$. After a 20-min incubation at 37°C, 190 μl of $DiSC_3(5)$-loaded cells was added to 2-fold dilutions of niclosamide, valinomycin, or nigericin in 96-well black clear-bottom plates (Corning, NY). Fluorescence (excitation [Ex], 620-nm wavelength; emission [Em], 685-nm wavelength) was immediately read using a Synergy H1 Hybrid plate reader. Niclosamide did not quench $DiSC_3$ in cell-free control assays.

Measurement of intracellular ATP levels. *E. coli* BW25113 was grown in MHB to early log phase ($OD_{600} = 0.2$) and then grown in the presence of niclosamide or carbonyl cyanide m-chlorophenylhydrazone (CCCP) for 60 min in clear flat-bottom 96-well plates. The OD_{600} was determined immediately before ATP levels were measured using BacTiter-Glo (Promega, Madison WI), according to the manufacturer's instructions. Relative ATP levels were calculated by dividing relative light units (RLU) by the OD_{600} (RLU/OD).

Measurement of oxygen consumption. *E. coli* strains were grown in MHB to early log phase ($OD_{600} = 0.4$) before dilution to $OD_{600} = 0.1$ prior to the assay. Diluted culture (50 μl) was added to individual wells of a 96-well black clear-bottom plate (Corning, NY) containing 5 μl of a DMSO control, CCCP, or niclosamide at the desired concentration and 5 μl of the MitoXpress oxygen probe. Cells were immediately covered with a layer of high-sensitivity mineral oil (50 μl) to restrict oxygen diffusion. Fluorescence (Ex, 380 nm; Em, 650 nm) was recorded using a Synergy H1 Hybrid plate reader.

Measurement of bacterial efflux. Subcultures of *E. coli* BW25113 were grown to early exponential phase (OD_{600} of ~0.4) in MHB supplemented with 5 mM EDTA, harvested by centrifugation, and resuspended in phosphate-buffered saline (PBS) to a final OD_{600} of 0.1. To initiate accumulation assays, Hoechst 33342 (1 μM) was added, cells were mixed by inversion, and 150-μl aliquots were added in a black, clear-bottom 96-well plate containing 50 μl of oxyclozanide, niclosamide, PAβN, or CCCP at 4× the

desired concentration(s) in PBS with 20% DMSO. Fluorescence (Ex, 355 nm; Em, 460 nm) was measured for 10 min using a Synergy H1 Hybrid plate reader (58).

Measurement of intrabacterial redox potential. roGFP contains an intramolecular disulfide bond that induces a shift in fluorescence emission between 405 nm and 480 nm; thus, intracellular oxidative stress can be ratiometrically monitored. *In vitro* analysis of the intrabacterial redox potential was performed as previously published (42). Assays were performed at 30°C in a Synergy H1 Hybrid plate reader with excitation measured at 405 and 480 nm and emission at 510 nm. Log-phase bacterial cultures were resuspended in 0.9% sodium chloride at an OD_{600} of 1.0, and 180 μl per well was loaded in a black, clear-bottom 96-well plate. The signals for fully oxidized or fully reduced bacteria were obtained by adding 5 mM H_2O_2 or 10 mM dithiothreitol (DTT) to the bacterial culture at the start of the experiment. Niclosamide was added at 1 and 0.1 $\mu g \cdot ml^{-1}$. All values were normalized to the values obtained for maximally oxidized and for fully reduced bacterial cultures.

AMNIS ImageStream and IDEAS/ImageJ analysis. Samples were analyzed by the use of an AMNIS ImageStream system as previously described (42). The laser intensities for wavelengths of 405, 488, 658, and 785 nm were 100, 120, 20, and 3.8, respectively. The data files were further analyzed with IDEAS software, version 6.0.129.0, which is supplied by AMNIS. Bacterial cells were selected based on fluorescence at 660 nm. Every cell image was then selected by the program based on fluorescent intensity at 660 nm. A mask was then created for analysis of the 405-nm/480-nm (405/480) ratio. The resulting 405/480 signals were plotted in a histogram. Reduced and oxidized controls were obtained within each experiment, and niclosamide was administered at 2 $\mu g \cdot ml^{-1}$. All values were normalized to oxidized and reduced ratio values. Pseudocolored ratio images were generated by ImageJ as described previously (42).

Murine abscess infection studies. Animal experiments were performed in accordance with The Canadian Council on Animal Care (CCAC) guidelines and were approved by the University of British Columbia Animal Care Committee (certificate number A14-0363). Mice used in this study were female outbred CD-1. All animals were purchased from Charles River Laboratories (Wilmington, MA), were 7 weeks of age, and weighed 25 $\pm$ 3 g at the time of the experiments. Isoflurane (1% to 3%) was used for anesthesia. Mice were euthanized with carbon dioxide. The abscess infection model was performed as previously described (53). *K. pneumoniae* KPLN649 and *P. aeruginosa* LESB58 were grown to an OD_{600} of 1.0 in double yeast tryptone (dYT) medium. Prior to injection, bacterial cells were washed twice with sterile PBS and resuspended to 5×10^7 CFU for *P. aeruginosa* LESB58 and to 1×10^9 CFU for *K. pneumoniae* KPLN649. A 50-μl bacterial suspension was injected into the right side of the dorsum. Up to 10 mg of niclosamide per kg of body weight and up to 5 $mg \cdot kg^{-1}$ colistin, each dissolved in 2.5% DMSO–42.5% polyethylene glycol 400 (PEG 400), were tested for skin toxicity prior to efficacy testing. Treatment was applied directly into the subcutaneous space into the infected area (50 μl) at 1 h postinfection. The progression of the disease/infection was monitored daily, and skin abscesses (including all accumulated pus) were excised on day 3 and homogenized in sterile PBS using a Mini-Beadbeater-96 cell disruptor (Biospec Products, Bartlesville, OK) for 5 min and bacterial counts determined by serial dilution. Experiments were performed at least 3 times independently with 3 to 4 animals per group.

SUPPLEMENTAL MATERIAL

Supplemental material is available online only.

FIG S1, TIF file, 0.2 MB.

FIG S2, TIF file, 0.9 MB.

FIG S3, TIF file, 0.7 MB.

FIG S4, TIF file, 10.5 MB.

FIG S5, TIF file, 1 MB.

FIG S6, TIF file, 1.1 MB.

TABLE S1, PDF file, 0.1 MB.

TABLE S2, PDF file, 0.1 MB.

TABLE S3, PDF file, 0.1 MB.

ACKNOWLEDGMENTS

This work was supported by the Royal Society of New Zealand Marsden Fund (grant VUW1502 to D.F.A.), the Health Research Council of New Zealand (18-532 to D.F.A.), a Natural Sciences and Engineering Research Council of Canada Discovery Grant (RGPIN 2017-04909 to N.T.), and a Canadian Institutes for Health Research (CIHR) grant (FDN-154287 to R.E.W.H.). D.P. received a Cystic Fibrosis Postdoctoral Fellowship (Canada) and a Research Trainee Award from the Michael Smith Foundation for Health Research. R.E.W.H. holds a Canada Research Chair in Health and Genomics and a UBC Killam Professorship. N.T. is a CIHR new investigator and a Michael Smith Foundation of Health Research career investigator.

J.N.C. thanks Jaiten Saini for technical support.

J.N.C. and D.F.A. designed and directed the project and cowrote the manuscript.

J.N.C. performed the mechanistic studies and bacterial screening assays. N.T. assisted project design and cowrote the manuscript. J.V.D.H. performed the AMNIS high-throughput screening and assisted intracellular redox assays; M.H.R., A.S.B., R.F.L., C.M.M., and R.J.E. assisted bacterial screening; E.M.W. provided experimental support for molecular engineering and bacterial assays; D.P. carried out all abscess infection studies; D.P. and R.E.W.H. directed the mouse abscess infection studies and assisted in manuscript editing.

J.N.C. and D.F.A. are coinventors on patent filings WO/2016/080846 and WO/2017/200396 for the application of niclosamide, and related compounds, in conjunction with efflux inhibitors or membrane permeabilizing agents. Some of the claims in these filings are supported by this work.

REFERENCES

1. World Health Organization. 2017. Global priority list of antibiotic-resistant bacteria to guide research, discovery, and development of new antibiotics. WHO, Geneva, Switzerland.
2. Tyers M, Wright GD. 2019. Drug combinations: a strategy to extend the life of antibiotics in the 21st century. Nat Rev Microbiol 17:141–155. https://doi.org/10.1038/s41579-018-0141-x.
3. Zimmer A, Katzir I, Dekel E, Mayo AE, Alon U. 2016. Prediction of multidimensional drug dose responses based on measurements of drug pairs. Proc Natl Acad Sci U S A 113:10442–10447. https://doi.org/10.1073/pnas.1606301113.
4. Yeh P, Tschumi AI, Kishony R. 2006. Functional classification of drugs by properties of their pairwise interactions. Nat Genet 38:489–494. https://doi.org/10.1038/ng1755.
5. Zuo GY, Li Y, Wang T, Han J, Wang GC, Zhang YL, Pan D. 2011. Synergistic antibacterial and antibiotic effects of bisbenzylisoquinoline alkaloids on clinical isolates of methicillin-resistant *Staphylococcus aureus* (MRSA). Molecules 16:9819–9826. https://doi.org/10.3390/molecules16129819.
6. Mitchison DA. 2012. Prevention of drug resistance by combined drug treatment of tuberculosis, p 87–98. *In* Coates A (ed), Antibiotic resistance. Handbook of experimental pharmacology, vol 211. Springer, Berlin, Germany. https://doi.org/10.1007/978-3-642-28951-4_6.
7. Vidaillac C, Benichou L, Duval RE. 2012. In vitro synergy of colistin combinations against colistin-resistant *Acinetobacter baumannii*, *Pseudomonas aeruginosa*, and *Klebsiella pneumoniae* isolates. Antimicrob Agents Chemother 56:4856–4861. https://doi.org/10.1128/AAC.05996-11.
8. Foucquier J, Guedj M. 2015. Analysis of drug combinations: current methodological landscape. Pharmacol Res Perspect 3:e00149. https://doi.org/10.1002/prp2.149.
9. Tooke CL, Hinchliffe P, Bragginton EC, Colenso CK, Hirvonen VHA, Takebayashi Y, Spencer J. 2019. β-Lactamases and β-lactamase inhibitors in the 21st century. J Mol Biol 431:3472–3500. https://doi.org/10.1016/j.jmb.2019.04.002.
10. Minato Y, Dawadi S, Kordus SL, Sivanandam A, Aldrich CC, Baughn AD. 2018. Mutual potentiation drives synergy between trimethoprim and sulfamethoxazole. Nat Commun 9:1003. https://doi.org/10.1038/s41467-018-03447-x.
11. Lehtinen J, Lilius EM. 2007. Promethazine renders *Escherichia coli* susceptible to penicillin G: real-time measurement of bacterial susceptibility by fluoro-luminometry. Int J Antimicrob Agents 30:44–51. https://doi.org/10.1016/j.ijantimicag.2007.02.019.
12. Kristiansen JE, Hendricks O, Delvin T, Butterworth TS, Aagaard L, Christensen JB, Flores VC, Keyzer H. 2007. Reversal of resistance in microorganisms by help of non-antibiotics. J Antimicrob Chemother 59:1271–1279. https://doi.org/10.1093/jac/dkm071.
13. Ejim L, Farha MA, Falconer SB, Wildenhain J, Coombes BK, Tyers M, Brown ED, Wright GD. 2011. Combinations of antibiotics and nonantibiotic drugs enhance antimicrobial efficacy. Nat Chem Biol 7:348–350. https://doi.org/10.1038/nchembio.559.
14. Konreddy AK, Rani GU, Lee K, Choi Y. 2019. Recent drug-repurposing-driven advances in the discovery of novel antibiotics. Curr Med Chem 26:5363–5388. https://doi.org/10.2174/0929867325666180706101404.
15. Stokes JM, MacNair CR, Ilyas B, French S, Côté J-P, Bouwman C, Farha MA, Sieron AO, Whitfield C, Coombes BK, Brown ED. 2017. Pentamidine sensitizes Gram-negative pathogens to antibiotics and overcomes acquired colistin resistance. Nat Microbiol 2:17028. https://doi.org/10.1038/nmicrobiol.2017.28.
16. Ditzel J, Schwartz M. 1967. Worm cure without tears. The effect of niclosamide on *Taeniasis saginata* in man. J Intern Med 182:663–664.
17. Chen W, Mook RA, Premont RT, Wang J. 2018. Niclosamide: beyond an antihelminthic drug. Cell Signal 41:89–96. https://doi.org/10.1016/j.cellsig.2017.04.001.
18. Weinbach EC, Garbus J. 1969. Mechanism of action of reagents that uncouple oxidative phosphorylation. Nature 221:1016–1018. https://doi.org/10.1038/2211016a0.
19. Kadri H, Lambourne OA, Mehellou Y. 2018. Niclosamide, a drug with many (re)purposes. ChemMedChem 13:1088–1091. https://doi.org/10.1002/cmdc.201800100.
20. Wu CJ, Jan JT, Chen CM, Hsieh HP, Hwang DR, Liu HW, Liu CY, Huang HW, Chen SC, Hong CF, Lin RK, Chao YS, Hsu JTA. 2004. Inhibition of severe acute respiratory syndrome coronavirus replication by niclosamide. Antimicrob Agents Chemother 48:2693–2696. https://doi.org/10.1128/AAC.48.7.2693-2696.2004.
21. Jeon S, Ko M, Lee J, Choi I, Byun SY, Park S, Shum D, Kim S. 2020. Identification of antiviral drug candidates against SARS-CoV-2 from FDA-approved drugs. bioRxiv https://doi.org/10.1101/2020.03.20.999730.
22. Jurgeit A, McDowell R, Moese S, Meldrum E, Schwendener R, Greber UF. 2012. Niclosamide is a proton carrier and targets acidic endosomes with broad antiviral effects. PLoS Pathog 8:e1002976. https://doi.org/10.1371/journal.ppat.1002976.
23. Rajamuthiah R, Fuchs BB, Conery AL, Kim W, Jayamani E, Kwon B, Ausubel FM, Mylonakis E. 2015. Repurposing salicylanilide anthelmintic drugs to combat drug resistant *Staphylococcus aureus*. PLoS One 10:e0124595. https://doi.org/10.1371/journal.pone.0124595.
24. Gooyit M, Janda KD. 2016. Reprofiled anthelmintics abate hypervirulent stationary-phase *Clostridium difficile*. Sci Rep 6:33642. https://doi.org/10.1038/srep33642.
25. Tharmalingam N, Port J, Castillo D, Mylonakis E. 2018. Repurposing the anthelmintic drug niclosamide to combat *Helicobacter pylori*. Sci Rep 8:3701. https://doi.org/10.1038/s41598-018-22037-x.
26. Andrews P, Thyssen J, Lorke D. 1982. The biology and toxicology of molluscicides, bayluscide. Pharmacol Ther 19:245–295. https://doi.org/10.1016/0163-7258(82)90064-X.
27. Lin CK, Bai MY, Hu TM, Wang YC, Chao TK, Weng SJ, Huang RL, Su PH, Lai HC. 2016. Preclinical evaluation of a nanoformulated antihelminthic, niclosamide, in ovarian cancer. Oncotarget 7:8993–9006. https://doi.org/10.18632/oncotarget.7113.
28. Mook RA, Wang J, Ren X-R, Chen M, Spasojevic I, Barak LS, Lyerly HK, Chen W. 2015. Structure-activity studies of Wnt/β-catenin inhibition in the niclosamide chemotype: identification of derivatives with improved drug exposure. Bioorg Med Chem 23:5829–5838. https://doi.org/10.1016/j.bmc.2015.07.001.
29. Costabile G, d'Angelo I, Rampioni G, Bondì R, Pompili B, Ascenzioni F, Mitidieri E, d'Emmanuele di Villa Bianca R, Sorrentino R, Miro A, Quaglia F, Imperi F, Leoni L, Ungaro F. 2015. Toward repositioning niclosamide for antivirulence therapy of *Pseudomonas aeruginosa* lung infections: development of inhalable formulations through nanosuspension technology. Mol Pharm 12:2604–2617. https://doi.org/10.1021/acs.molpharmaceut.5b00098.
30. Ayerbe-Algaba R, Gil-Marqués ML, Jiménez-Mejías ME, Sánchez-

Encinales V, Parra-Millán R, Pachón-Ibáñez ME, Pachón J, Smani Y. 2018. Synergistic activity of niclosamide in combination with colistin against colistin-susceptible and colistin-resistant *Acinetobacter baumannii* and *Klebsiella pneumoniae*. Front Cell Infect Microbiol 8:348. https://doi.org/10.3389/fcimb.2018.00348.

31. Domalaon R, De Silva PM, Kumar A, Zhanel GG, Schweizer F. 2019. The anthelmintic drug niclosamide synergizes with colistin and reverses colistin resistance in Gram-negative bacilli. Antimicrob Agents Chemother 63:e02574-18. https://doi.org/10.1128/AAC.02574-18.
32. Ackerley DF, Copp JN. 2017. Antibacterial compositions. Patent WO2016080846A1.
33. Pletzer D, Mansour SC, Wuerth K, Rahanjam N, Hancock REW. 2017. New mouse model for chronic infections by Gram-negative bacteria enabling the study of anti-infective efficacy and host-microbe interactions. mBio 8:e00140-17. https://doi.org/10.1128/mBio.00140-17.
34. Tal N, Schuldiner S. 2009. A coordinated network of transporters with overlapping specificities provides a robust survival strategy. Proc Natl Acad Sci U S A 106:9051–9056. https://doi.org/10.1073/pnas.0902400106.
35. Ryan A. 2017. Azoreductases in drug metabolism. Br J Pharmacol 174:2161–2173. https://doi.org/10.1111/bph.13571.
36. Akiva E, Copp JN, Tokuriki N, Babbitt PC. 2017. Evolutionary and molecular foundations of multiple contemporary functions of the nitroreductase superfamily. Proc Natl Acad Sci U S A 114:E9549–E9558. https://doi.org/10.1073/pnas.1706849114.
37. Fonseca BD, Diering GH, Bidinosti MA, Dalal K, Alain T, Balgi AD, Forestieri R, Nodwell M, Rajadurai CV, Gunaratnam C, Tee AR, Duong F, Andersen RJ, Orlowski J, Numata M, Sonenberg N, Roberge M. 2012. Structure-activity analysis of niclosamide reveals potential role for cytoplasmic pH in control of mammalian target of rapamycin complex 1 (mTORC1) signaling. J Biol Chem 287:17530–17545. https://doi.org/10.1074/jbc.M112.359638.
38. Prosser GA, Copp JN, Syddall SP, Williams EM, Smaill JB, Wilson WR, Patterson AV, Ackerley DF. 2010. Discovery and evaluation of Escherichia coli nitroreductases that activate the anti-cancer prodrug CB1954. Biochem Pharmacol 79:678–687. https://doi.org/10.1016/j.bcp.2009.10.008.
39. Bussy U, Chung-Davidson YW, Li K, Li W. 2014. Phase I and phase II reductive metabolism simulation of nitro aromatic xenobiotics with electrochemistry coupled with high resolution mass spectrometry. Anal Bioanal Chem 406:7253–7260. https://doi.org/10.1007/s00216-014-8171-3.
40. Yadav B, Wennerberg K, Aittokallio T, Tang J. 2015. Searching for drug synergy in complex dose-response landscapes using an interaction potency model. Comput Struct Biotechnol J 13:504–513. https://doi.org/10.1016/j.csbj.2015.09.001.
41. Hurdle JG, O'Neill AJ, Chopra I, Lee RE. 2011. Targeting bacterial membrane function: an underexploited mechanism for treating persistent infections. Nat Rev Microbiol 9:62–75. https://doi.org/10.1038/nrmicro2474.
42. van der Heijden J, Bosman ES, Reynolds LA, Finlay BB. 2015. Direct measurement of oxidative and nitrosative stress dynamics in Salmonella inside macrophages. Proc Natl Acad Sci U S A 112:560–565. https://doi.org/10.1073/pnas.1414569112.
43. Lamers RP, Cavallari JF, Burrows LL. 2013. The efflux inhibitor phenylalanine-arginine beta-naphthylamide (PAβN) permeabilizes the outer membrane of Gram-negative bacteria. PLoS One 8:e60666. https://doi.org/10.1371/journal.pone.0060666.
44. Anes J, McCusker MP, Fanning S, Martins M. 2015. The ins and outs of RND efflux pumps in *Escherichia coli*. Front Microbiol 6:587. https://doi.org/10.3389/fmicb.2015.00587.
45. Zlitni S, Ferruccio LF, Brown ED. 2013. Metabolic suppression identifies new antibacterial inhibitors under nutrient limitation. Nat Chem Biol 9:796–804. https://doi.org/10.1038/nchembio.1361.
46. Velkov T, Roberts KD, Thompson PE, Li J. 2016. Polymyxins: a new hope in combating Gram-negative superbugs? Future Med Chem 8:1017–1025. https://doi.org/10.4155/fmc-2016-0091.
47. Delavenne EFA, Simon DJJ, Sommer MOA, Toft-Kehler RV, Aps A. 2016. Antibacterial use of halogenated salicylanilides. Patent WO2016038035A1.
48. Farha MA, Verschoor CP, Bowdish D, Brown ED. 2013. Collapsing the proton motive force to identify synergistic combinations against *Staphylococcus aureus*. Chem Biol 20:1168–1178. https://doi.org/10.1016/j.chembiol.2013.07.006.
49. Feng X, Zhu W, Schurig-Briccio LA, Lindert S, Shoen C, Hitchings R, Li J, Wang Y, Baig N, Zhou T, Kim BK, Crick DC, Cynamon M, McCammon JA, Gennis RB, Oldfield E. 2015. Antiinfectives targeting enzymes and the proton motive force. Proc Natl Acad Sci U S A 112:E7073–E7082. https://doi.org/10.1073/pnas.1521988112.
50. Goodwin A, Kersulyte D, Sisson G, Veldhuyzen van Zanten SJ, Berg DE, Hoffman PS. 1998. Metronidazole resistance in *Helicobacter pylori* is due to null mutations in a gene (rdxA) that encodes an oxygen-insensitive NADPH nitroreductase. Mol Microbiol 28:383–393. https://doi.org/10.1046/j.1365-2958.1998.00806.x.
51. Baba T, Ara T, Hasegawa M, Takai Y, Okumura Y, Baba M, Datsenko KA, Tomita M, Wanner BL, Mori H. 2006. Construction of *Escherichia coli* K-12 in-frame, single-gene knockout mutants: the Keio collection. Mol Syst Biol 2:2006.0008. https://doi.org/10.1038/msb4100050.
52. Copp JN, Williams EM, Rich MH, Patterson AV, Smaill JB, Ackerley DF. 2014. Toward a high-throughput screening platform for directed evolution of enzymes that activate genotoxic prodrugs. Protein Eng Des Sel 27:399–403. https://doi.org/10.1093/protein/gzu025.
53. Pletzer D, Mansour SC, Hancock REW. 2018. Synergy between conventional antibiotics and anti-biofilm peptides in a murine, sub-cutaneous abscess model caused by recalcitrant ESKAPE pathogens. PLoS Pathog 14:e1007084. https://doi.org/10.1371/journal.ppat.1007084.
54. Akhoundsadegh N, Belanger CR, Hancock REW. 2019. Outer membrane interaction kinetics of new polymyxin B analogs in Gram-negative bacilli. Antimicrob Agents Chemother 63:e00935-19. https://doi.org/10.1128/AAC.00935-19.
55. Wiegand I, Hilpert K, Hancock REW. 2008. Agar and broth dilution methods to determine the minimal inhibitory concentration (MIC) of antimicrobial substances. Nat Protoc 3:163–175. https://doi.org/10.1038/nprot.2007.521.
56. Copp JN, Mowday AM, Williams EM, Guise CP, Ashoorzadeh A, Sharrock AV, Flanagan JU, Smaill JB, Patterson AV, Ackerley DF. 2017. Engineering a multifunctional nitroreductase for improved activation of prodrugs and PET probes for cancer gene therapy. Cell Chem Biol 24:391–403. https://doi.org/10.1016/j.chembiol.2017.02.005.
57. Ianevski A, He L, Aittokallio T, Tang J. 2017. SynergyFinder: a Web application for analyzing drug combination dose-response matrix data. Bioinformatics 33:2413–2415. https://doi.org/10.1093/bioinformatics/btx162.
58. Coldham NG, Webber M, Woodward MJ, Piddock LJV. 2010. A 96-well plate fluorescence assay for assessment of cellular permeability and active efflux in *Salmonella enterica* serovar *Typhimurium* and *Escherichia coli*. J Antimicrob Chemother 65:1655–1663. https://doi.org/10.1093/jac/dkq169.